Van Paepegem, W. and Degrieck, J. (2002). Tensile and Compressive Damage Coupling for Fully-reversed Bending Fatigue of Fibre-reinforced Composites. *Fatigue and Fracture of Engineering Materials & Structures*, 25(6), 547-562.

Tensile and Compressive Damage Coupling for Fully-reversed Bending Fatigue of Fibre-reinforced Composites

W. VAN PAEPEGEM* and J. DEGRIECK

Ghent University, Dept. of Mechanical Construction and Production, Sint-Pietersnieuwstraat 41, B-9000 Gent, Belgium

ABSTRACT Due to their high specific stiffness and strength, fibre-reinforced composite materials are winning through in a wide range of applications in automotive, naval and aerospace industy. Their design for fatigue is a complicated problem and a large research effort is being spent on it today. However there is still a need for extensive experimental testing or large safety factors to be adopted, because numerical simulations of the fatigue damage behaviour of fibre-reinforced composites are often found to be unreliable. This is due to the limited applicability of the theoretical models developed so far, compared to the complex multi-axial fatigue loadings that composite components often have to sustain in in-service loading conditions.

In this paper a new phenomenological fatigue model is presented. It is basically a residual stiffness model, but through an appropriate choice of the stress measure, the residual strength and thus final failure can be predicted as well. Two coupled growth rate equations for tensile and compressive damage describe the damage growth under tension-compression loading conditions and provide a much more general approach than the use of the stress ratio R. The model has been applied to fully-reversed bending of plain woven glass/epoxy specimens. Stress redistributions and the three stages of stiffness degradation (sharp initial decline – gradual deterioration – final failure) could be simulated satisfactorily.

Keywords fatigue; composites; residual stiffness; tension-compression.

INTRODUCTION

Fibre-reinforced composite materials are finding more and more applications in automotive, naval and aerospace industry. They have quite a good rating as regards to life time in fatigue, but the same does not apply to the number of cycles to initial damage. Although the fatigue behaviour of fibre-reinforced composites has been studied for many years, it is so diverse and complex that present knowledge is far from complete.

Moreover the design experience with metals cannot be simply transposed to the design of composites, because composites are inhomogeneous and anisotropic in nature. There are a number of important differences between the fatigue behaviour of metals and of fibre-reinforced composites. In metals, the stage of gradual and invisible deterioration spans nearly

* Corresponding author (Fax: +32-(0)9-264.35.87, E-mail: Wim.VanPaepegem@rug.ac.be).

the whole fatigue life time. No significant reduction of stiffness is observed in metals during the fatigue process. The final stage of the process starts with the formation of small cracks, which are the only form of macroscopically observable damage. Gradual growth and coalescence of these cracks quickly produce a large crack and final failure of the structural component.

Fibre-reinforced polymers are made of reinforcing fibres embedded in a polymer matrix. This makes them heterogeneous and anisotropic. The first stage of deterioration by fatigue is observable by the formation of damage zones, which contain a multitude of microscopic cracks and other forms of damage, such as debonding and pull-out of fibres from the matrix. It is important to observe that damage starts very early, after only a few or a few hundred loading cycles. This early damage is followed by a second stage of very gradual deterioration of the material, characterized by a gradual reduction of the stiffness. More serious types of damage appear in the third stage, such as fibre breakage and unstable delamination growth, leading to an accelerated decline and final failure.

These major differences in damage behaviour must be reflected in the modelling approach. Indeed, as the stiffness of a metal remains quasi unaffected during fatigue life, the linear relation between stress and strain remains valid. Although more and more complicated fatigue laws for metals are developed due to their complex material design and the severe in-service fatigue loadings, the fatigue process can still be simulated in most common cases by one finite element calculation. Then in the post-processing stage, the fatigue life of the individual nodes of the finite element mesh is assessed taking into account the (multi-axial) stress state in that particular node. Often the critical plane concept is used for this purpose [1].

On the contrary, the gradual deterioration of a fibre-reinforced composite can lead to continuous stress redistributions during fatigue life, and a reduction of stress concentrations in a structural component. To simulate these stress redistributions accurately, the simulation should follow the path of successive damage states and evaluate the changing stiffness distribution at regular times during fatigue life.

Fatigue models for fibre-reinforced composites can be generally classified into three categories [2]: (i) fatigue life models, which do not take into account the actual degradation mechanisms but use S-N curves or Goodman-type diagrams and introduce some sort of fatigue failure criterion; (ii) phenomenological models for residual stiffness/strength; and (iii) progressive damage models which use one or more damage variables related to measurable manifestations of damage (transverse matrix cracks, delamination size).

As reported earlier by the authors [3][4], stress redistribution can indeed be an important phenomenon with experimental fatigue testing, and hence the residual stiffness approach was chosen as the basis of the present model. Such residual stiffness models propose an evolution law which describes the (gradual) deterioration of the stiffness of the composite specimen in terms of macroscopically observable properties. As a consequence they are able to simulate stress redistribution. Moreover stiffness can be measured nondestructively and the scatter is small. On the other hand, residual stiffness models have no distinct criterion for fatigue failure as compared to residual strength models. Fatigue failure is most often assumed to occur when the modulus has degraded to a critical level which is not unique and has been defined by many investigators. Already in the early 70s, Salkind [5] suggested to draw a family of S-N curves, being contours of a specified percentage of stiffness loss, to present fatigue data. Hahn and Kim [6] and O'Brien and Reifsnider [7] proposed that fatigue failure occurs when the fatigue secant modulus degrades to the secant modulus at the moment of failure in a static test. According to Hwang and Han [8], fatigue failure occurs when the fatigue resultant strain reaches the ultimate static strain.

To alleviate this problem, the static Tsai-Wu failure criterion will be used in a different way in the present model. It will provide a measure for the applied fatigue stress level, but with a

correlation to the remaining strength. This coupled model of residual stiffness and strength can simulate the three stages of stiffness degradation: sharp initial decline, gradual deterioration and final failure.
Further the damage growth rate equation will be split up in two differential equations, describing the development of tensile and compressive damage, respectively. Through the coupling of these two equations, the aggravating effect of fully-reversed tension-compression fatigue loadings can be simulated.

MATERIALS AND EXPERIMENTAL SETUP

The material used in the fatigue experiments, was a glass fabric/epoxy composite. The fabric was a Roviglass R420 plain woven glass fabric (Syncoglas) and the epoxy was Araldite LY 556 (Ciba-Geigy). The plain woven glass fabric was stacked in eight layers, denoted as $[\#0^o]_8$, where '0°' means that the warp direction of each of the eight layers has been aligned with the loading direction and where the symbol '#' refers to the fabric reinforcement type. All composite specimens were manufactured using the resin-transfer-moulding technique. After curing they had a thickness of 2.72 mm. The samples were cut to dimensions of 145 mm long by 30 mm wide on a water-cooled diamond saw. The fibre volume fraction V_f was 0.48. The in-plane elastic properties of the $[\#0°]_8$ composite laminates were determined using the dynamic modal analyis method described by Sol et al. [9][10], while the static tensile strength X_T and compressive strength X_C were determined with an Instron hydraulic testing machine (ASTM D 3039). All relevant material properties are listed in Table 1.

Table 1 Measured in-plane properties of the $[\#0°]_8$ composite laminates

E_{11} [GPa]	24.57
E_{22} [GPa]	23.94
ν_{12} [-]	0.153
G_{12} [GPa]	4.83
X_T [MPa]	390.7
X_C [MPa]	345.1

The experimental results were obtained from displacement-controlled cantilever bending fatigue experiments. One side of the specimen was clamped, while a sinusoidal displacement was imposed at the other side of the specimen. Figure 1 shows a schematic drawing.

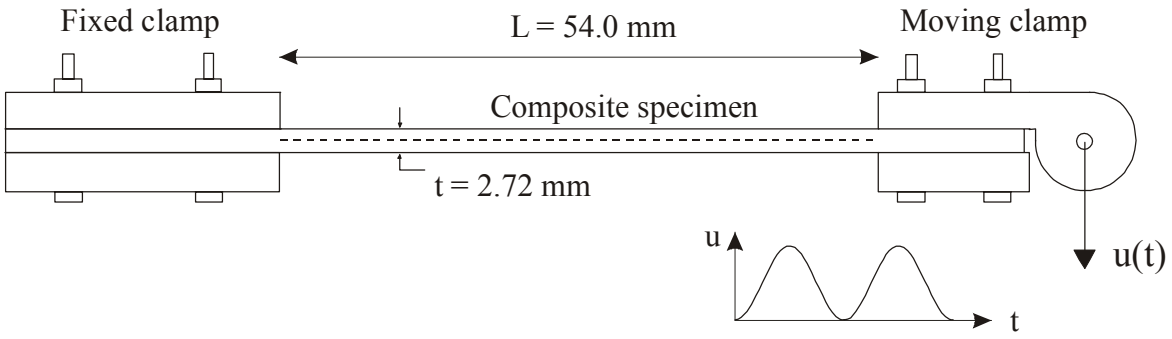

Figure 1 Schematic drawing of the bending fatigue setup.

The testing frequency for all fatigue experiments was 2.2 Hz. The amplitude u_{max} of the imposed displacement is a controllable parameter and the displacement ratio R_d (analogous to the stress ratio R) is defined as $R_d = u_{min}/u_{max}$. For single-sided bending $R_d = 0.0$, while for fully-reversed bending $R_d = -1.0$. Of course, due to the varying bending moment along the specimen length and the varying stresses and strains along the specimen length and through its thickness, the maximum stress amplitude can be different in each material point.

FATIGUE DAMAGE MODEL FOR SINGLE-SIDED BENDING

Recently the authors have proposed a phenomenological fatigue damage model for uni-axial loading conditions [11][12]. This model was developed for single-sided bending and did not take into account the effect of negative displacement ratios R_d (or equivalent: negative stress ratios R). This model will first be explained and then be extended for negative stress ratios (tension-compression fatigue loading).

Definition of the fatigue failure index Σ(σ, D)

As mentioned earlier, the modified interpretation of the static Tsai-Wu failure criterion must provide a stress value, which is a measure for the actually applied stress amplitude in the considered material point, but now in relation with the composite's actual strength.
To that purpose, the definition of the failure index, as proposed by Liu and Tsai [13], is recalled here. The failure index is the inverse value of the strength factor Φ, the latter being the reserve to failure in the static Tsai-Wu failure criterion. The strength (or safety) factor Φ is calculated from the Tsai-Wu equation as follows:

$$\left(\sigma^2 \frac{1}{X_T \cdot |X_C|}\right)\Phi^2 + \left[\sigma\left(\frac{1}{X_T} - \frac{1}{|X_C|}\right)\right]\Phi - 1 = 0 \tag{1}$$

where X_T and X_C are the static tensile and compressive strength and the strength ratio Φ defines the reserve factor to failure. If Φ = 1, failure occurs, while if for example Φ = 2, the factor of safety is 2. The failure index Σ(σ) is then defined as 1/Φ.
To use this criterion for fatigue modelling, the effective stress $\tilde{\sigma}$ is used. This stress measure originates from the continuum damage mechanics theory and is defined as:

$$\tilde{\sigma} = \frac{\sigma}{1 - D} = E_0 \varepsilon \tag{2}$$

where, for uni-axial loading conditions, the damage variable D represents the degradation of the longitudinal stiffness E_0 ($D = 1 - E/E_0$), σ is the applied nominal stress and ε is the nominal strain. When D is now considered as a measure for fatigue damage, the applied nominal stress σ is replaced by the effective stress $\tilde{\sigma}$ in the Equation (1) for calculation of the strength factor Φ:

$$\left[\left(\frac{\sigma}{1 - D}\right)^2 \frac{1}{X_T \cdot |X_C|}\right]\Phi^2 + \left[\frac{\sigma}{1 - D}\left(\frac{1}{X_T} - \frac{1}{|X_C|}\right)\right]\Phi - 1 = 0 \tag{3}$$

Thus, the failure index Σ becomes a function $\Sigma(\sigma, D)$ of both the applied nominal stress amplitude σ and the fatigue damage D. It could be argued that the use of the constant static strength instead of the fatigue strength in the definition of the fatigue failure index $\Sigma(\sigma, D)$, could lead to non-conservative predictions. However, there is an indirect relation with residual strength. In the one-dimensional case, it can be easily calculated that:

$$\Sigma(\sigma, D) = \frac{1}{\Phi} = \frac{\tilde{\sigma}}{X} = \frac{\frac{\sigma}{1-D}}{X} = \frac{E_0 \varepsilon}{X} \qquad (X = X_T, X_C) \tag{4}$$

Thus, in the one-dimensional case, the proposed definition of the fatigue failure index $\Sigma(\sigma, D)$ is equivalent with the ratio of the applied nominal stress σ to the residual strength $X \cdot (1-D)$ ($X = X_T, X_C$), because the effective stress $\tilde{\sigma}$ is defined as $\sigma/(1-D)$ (Equation (2)). The only difference is the interpretation of the residual strength concept: here, it is assumed that the apparent loss of strength is due to the fact that the actual load-bearing area is decreased due to fatigue damage, and that the effective stress $\tilde{\sigma}$ in that cross-section is raised. If the effective stress $\tilde{\sigma}$ then equals the static strength X_T or X_C, the safety factor Φ and the fatigue failure index $\Sigma(\sigma, D)$ both equal 1.0 and final failure occurs for that particular material point. The advantage of this approach is that the introduction of the strength properties into the fatigue model does not require any new laws for residual strength to be established. The effective stress $\tilde{\sigma}$ is used to account for present fatigue damage.
Further, as the effective stress $\tilde{\sigma}$ equals $E_0 \cdot \varepsilon$ (Equation (2)), the fatigue failure index $\Sigma(\sigma, D)$ is also a measure for the applied fatigue strain.

Constitutive equations

From Equation (2), the damage D is defined as a measure for the stiffness degradation, lying between *zero* (undamaged material) and *one* (complete failure). The remaining equation to complete the fatigue damage model, is the damage growth rate equation dD/dN, where N is the cycle number. This fatigue model has been recently proposed by the authors and its derivation can be found in detail in reference [12]. The model distinguishes between a growth rate for tensile stresses ($\sigma \geq 0$) and one for compressive stresses ($\sigma < 0$) [11][12]:

$$\frac{dD}{dN} = \begin{cases} \underbrace{c_1 \cdot \Sigma \cdot \exp\left(-c_2 \frac{D}{\sqrt{\Sigma}}\right)}_{\text{initiation}} + \underbrace{c_3 \cdot D \cdot \Sigma^2 \cdot \left[1 + \exp\left(c_5 (\Sigma - c_4)\right)\right]}_{\text{propagation}} & \text{if } \sigma \geq 0 \\ \underbrace{\left[c_1 \cdot \Sigma \cdot \exp\left(-c_2 \frac{D}{\sqrt{\Sigma}}\right)\right]^3}_{\text{initiation}} + \underbrace{c_3 \cdot D \cdot \Sigma^2 \cdot \left[1 + \exp\left(\frac{c_5}{3}(\Sigma - c_4)\right)\right]}_{\text{propagation}} & \text{if } \sigma < 0 \end{cases} \tag{5}$$

Both growth rate equations consist of two terms, separately accounting for damage initiation and damage propagation. If damage is very small, the second term is negligible ($D \approx 0$) and only the first initiation term is acting, while for larger values of D, the exponential function in the first term forces this term to diminish, while the second term is increasingly dominating. The damage initiation rate is different in tension and compression, because it was observed from the experimental fatigue tests that the compressive damage initiation rate is much smaller under the following restrictive conditions:

- the displacement ratio $R_d = 0.0$, which means that the bending experiments are single-sided. As a consequence, each material point is subjected to stresses which do not change sign during one cycle. Because $u_{min} = 0.0$, the stress ratio R is zero for all the material points involved,
- there are no delaminations. Due to the chosen stacking sequence, no delaminations have been observed during fatigue loading. It was a deliberate choice to exclude delaminations from the scope of modelling for the moment, because it would be nearly impossible to distinguish between the contribution of each damage type to the bending fatigue degradation of the studied material, especially in fully-reversed bending.

All five constants c_i ($i = 1,\ldots, 5$) in the fatigue damage model have a distinctive meaning:

- c_1 regulates the growth rate of the damage initiation regime (and thus the sharp initial decline of the modulus degradation curve),
- c_2 is sufficiently large, so that the first term is disappearing when damage increases. Then, the "Characteristic Damage State" of matrix cracking [14][15][16] has been reached,
- c_3 represents the growth rate in the second stage of modulus degradation, where additional damage mechanisms (fibre/matrix interface failure, fibre pull-out) lead to a gradual decline of the stiffness,
- c_4 and c_5 express the explosive damage growth once that the fatigue failure index $\Sigma(\sigma, D)$ approaches its failure value 1.0. Indeed, if the fatigue failure index crosses the threshold c_4, the power of the exponential function changes from negative to positive, causing a fast accelerating damage growth. In this stage, fibre fracture initiates and quickly localizes to cause final failure.

This fatigue damage model has been implemented in the commercial finite element code SAMCEF™. The integration of the damage growth rate equation for each Gauss-point of the finite element mesh has been done with the *cycle jump* approach which has also been recently proposed by the authors [17]. Briefly the *cycle jump* approach means that the computation is done for a certain set of loading cycles at deliberately chosen intervals, and that the effect on the stiffness degradation of these loading cycles is extrapolated over the corresponding intervals in an appropriate manner. To this purpose, each Gauss-point has been assigned – beside the damage variable D – a second state variable NJUMP1, which is the number of cycles over which extrapolation of the damage D is possible without losing reliability and accuracy for that particular Gauss-point. This local *cycle jump* NJUMP1 is calculated by imposing a maximum allowed increase in damage ΔD for each particular Gauss-point when the extrapolation would proceed for NJUMP1 cycles. When the increase ΔD is limited to for example 0.01, this is equivalent to a piecewise integration of the damage evolution law for that Gauss-point by dividing the ordinate axis of the damage-cycle history into 100 segments.

After looping over all Gauss-points, a cumulative relative frequency distribution of the NJUMP1 values is calculated and the overall *cycle jump* NJUMP (which will be applied to the whole finite element mesh) is determined as a percentile of this frequency distribution. By decreasing the upper threshold for ΔD for each Gauss-point, the damage evolution law dD/dN will be integrated more accurately, but the global NJUMP – a percentile of the cumulative frequency distribution of all NJUMP1 values – will be smaller and the calculation will proceed more slowly.

As such, the differential equation dD/dN is integrated for each Gauss-point of the finite element mesh, but depending on the loading conditions, the fatigue failure index $\Sigma(\sigma, D)$ can be different for each Gauss-point, and hence the damage growth rate dD/dN. After each *cycle jump*, the simulation of the fatigue loading cycle is restarted with altered damage and stiffness distributions in the composite structure. As a consequence, stress redistributions and relaxations of stress concentrations due to damage development can be accounted for by simulating the successive damage states.

The parameters c_i (i=1,…,5) in Equation (5) were determined for the bending fatigue test Pr05_2 which shows a clear distinction between the three stages in (bending) stiffness degradation: sharp initial decline, gradual (almost linear) reduction, and final accelerated decline. Since the fatigue damage model is not at all a curve-fitting model, the values of the constants c_i (i=1,…,5) were of course retained when simulating other loading conditions. Figure 2 shows the experimental and simulated force-cycle history for the Pr05_2 experiment. The imposed displacement varied between zero (stress ratio R = 0 for all Gauss-points) and u_{max} = 30.4 mm. The force was experimentally measured by a strain gauge bridge and represents the force necessary to impose the bending displacement with constant amplitude u_{max}. Due to the (bending) stiffness degradation, this force decreases during fatigue life.

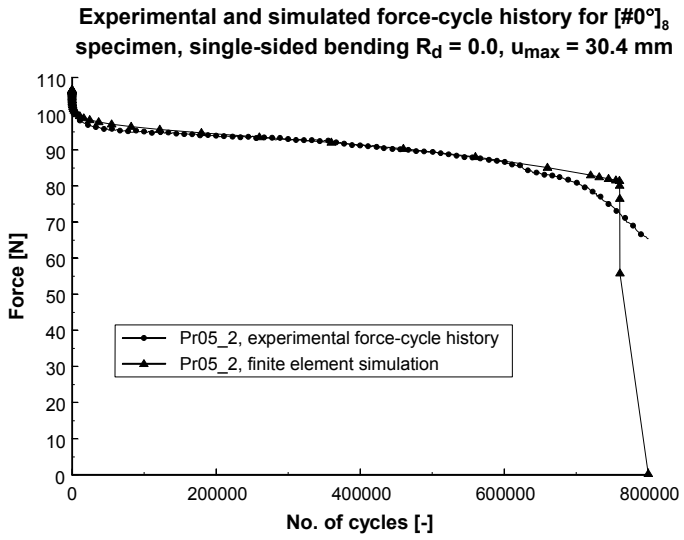

Figure 2 Experimental and simulated force-cycle history for single-sided bending (u_{max} = 30.4 mm).

The model parameters were determined with a non-linear optimization procedure. The determination of the parameters c_i (i=1,…,5) can be split up in two parts in order to reduce the optimization time. Indeed, since the damage initiation function should be able to account for the initial stiffness degradation, the first sharp decline of the force-cycle history can be used to determine the parameters c_1 and c_2. Then the parameters c_3, c_4 and c_5 can be determined for the full force-cycle history. The non-linear optimization procedure iteratively calls the finite element code, and optimizes the error between the experimentally measured force-cycle history and the predicted one for a predetermined number of loading cycles.
The final values of all constants in the model are listed in Table 2.

Table 2 Model constants.

c_1 [1/cycle]	0.002
c_2 [-]	30.0
c_3 [1/cycle]	$4.0 \cdot 10^{-6}$
c_4 [-]	0.85
c_5 [-]	93.0

It is important to note that the application of the fatigue damage model (Eq. (5)) is not limited to the simulation of bending experiments. As the fatigue model pretends to be a true material model, i.e. intrinsic to the material used, it predicts the stiffness degradation in each material point for the applied uni-axial nominal stress σ which can change during fatigue life and which might be different in each material point. However bending fatigue experiments were preferred because each material point through the thickness sustains a different stress amplitude σ (due to the bending moment), so that the fatigue damage model is tested for a wide range of tensile and compressive stress amplitudes. Moreover, due to the stress redistribution, the stress amplitude in the material points changes during fatigue life, and a sort of variable-amplitude loading is simulated. These advantages support the choice of the bending experiments as a powerful validation experiment for the model developed. The same arguments apply for the extended damage model for fully-reversed bending which will be outlined below.

EXTENSION OF THE MODEL FOR FULLY-REVERSED BENDING

For fully-reversed bending, the displacement ratio $R_d = -1.0$ and as a consequence, the applied stress amplitude changes sign during one fatigue loading cycle. It has been often reported in literature that this sign reversal of the applied stress has a devastating effect on fatigue life [18][19][20][21][22]. Indeed, in Figure 3 the experimental force-cycle history of the single-sided bending test Pr05_2 (see also Figure 2) is compared with the experimental force-cycle history of the fully-reversed bending test Pr08_6. For the single-sided bending test (u_{max} = 30.4 mm), the fatigue life was about 700,000 cycles. When fully-reversed bending was applied with even a lower displacement amplitude (u_{max} = 27.0 mm), the fatigue life was drastically reduced with a factor 10 to about 70,000 cycles.

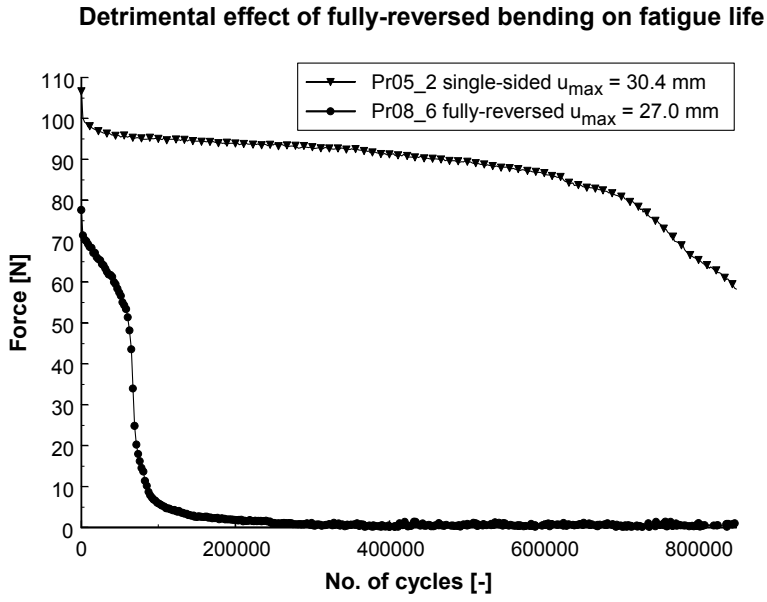

Figure 3 Comparison of experimental data from single-sided and fully-reversed bending tests.

When the fatigue damage model for single-sided bending (Eq. (5)) is applied to this fully-reversed bending fatigue experiment Pr08_6, the fatigue life is considerably overestimated,

because the interacting effects of tensile and compressive damage have not been included in the growth rate equations so far. Figure 4 illustrates the experimental and simulated results.

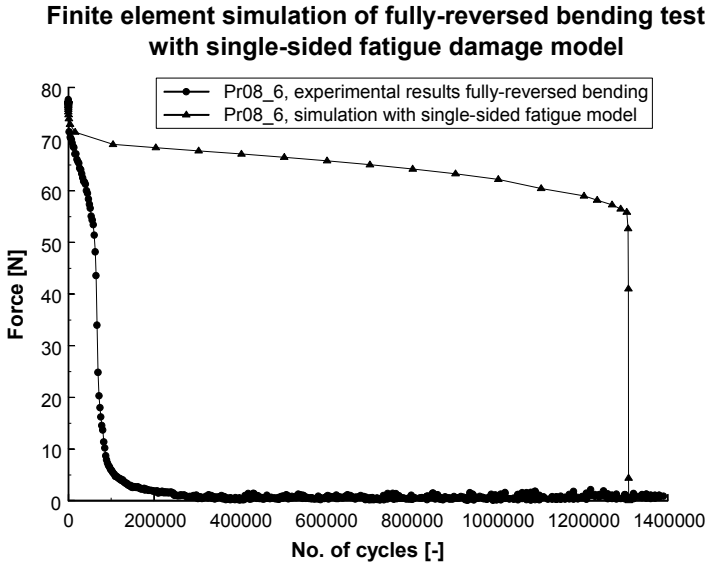

Figure 4 Simulation of the fully-reversed bending fatigue experiment with the fatigue damage model for single-sided bending.

The overestimation can be easily explained by the fact that in the single-sided bending model, the compressive part of the loading cycle causes negligible damage, due to the third power of the damage initiation function for compressive stresses (Eq. (5)). So only the tensile part of the loading cycle causes damage, and as u_{max} (= 27.0 mm) for the fully-reversed fatigue test is smaller than u_{max} (= 30.4 mm) for the experiment in Figure 2, the fatigue life must be longer than the fatigue life of 700,000 cycles which was predicted and experimentally observed for the fatigue test in Figure 2.
Therefore the fatigue damage model has been extended to include the interacting effect of tensile and compressive damage. First the general modelling framework for reversed fatigue loadings will be explained, based on the continuum damage mechanics theory. Secondly, the modified growth rate equations will be investigated in detail.

General modelling framework

The common fatigue modelling approach makes use of the stress ratio $R = \sigma_{min}/\sigma_{max}$ to characterize the nature of the fatigue test (tension-tension, tension-compression, compression-compression,…). In the authors' opinion, this approach is not generally suited, for several reasons:

- the stress ratio is only valid as a characterizing parameter of the fatigue test when uni-axial tension, compression or tension-compression tests are performed. In more complicated uni-axial loading conditions (e.g. bending), the stress ratio can be different for each material point and due to stress redistribution, the stress ratio for one particular material point can even change during fatigue life. For multi-axial loading conditions, the use of one single stress ratio does lose its sense completely, because the definition of a minimum and maximum stress level makes no sense,

- the stress ratio does not take into account the underlying damage mechanisms. A fatigue damage model should be based on a sound modelling of the actual damage kinetics in order to correctly model the detrimental interaction between tensile and compressive damage.

Therefore it is proposed here that the tension-compression fatigue loading cycle *for each material point* should be treated as two separate loading cycles, one in the tensile regime and one in the compressive regime, whereby the mutual interaction between these two loading cycles will be determined by the nature of the damage that is already present. In Figure 5 the principle is illustrated for a particular material point that is subjected to a tension-compression loading cycle. Of course, for other material points in the structure, the sequence might be compression-tension instead of tension-compression.

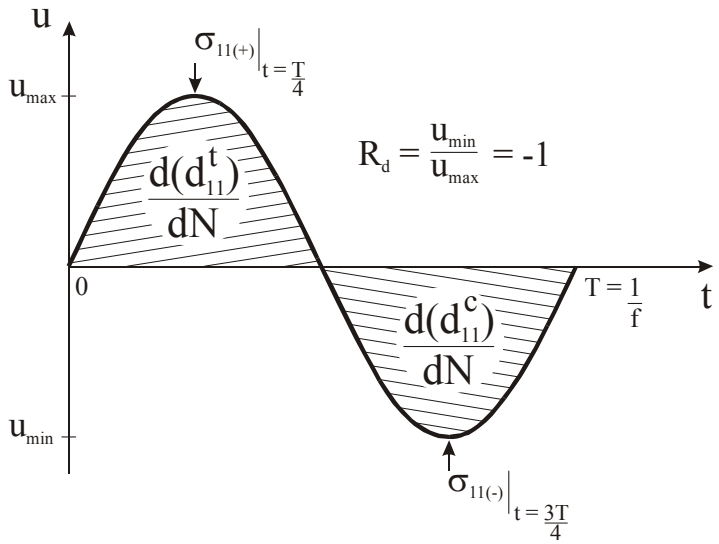

Figure 5 Interpretation of the tension-compression fatigue loading cycle.

For each material point, the uni-axial damage variable D (further designated as D_{11}) is discriminated into d_{11}^t (damage caused by tensile stresses) and d_{11}^c (damage caused by compressive stresses). The sum of both contributions d_{11}^t and d_{11}^c still equals the total damage D_{11}. In Figure 5 the first half of the loading cycle is in the tensile regime and the maximum tensile stress is $\sigma_{11(+)}$ (t = T/4) where T is the period of the full tension-compression loading cycle; the corresponding growth rate is $d(d_{11}^t)/dN$. In the second loading cycle the maximum compressive stress is $\sigma_{11(-)}$ (t = 3T/4) and the corresponding growth rate is $d(d_{11}^c)/dN$. The exact expression for these growth rate equations will be discussed further. Next, a new fatigue loading cycle must be evaluated with altered damage state and stiffness distribution. The *cycle jump* approach [17] still remains valid. From the maximum allowed increase for D_{11} (= $d_{11}^t + d_{11}^c$), the local *cycle jump* is estimated for each Gauss-point of the finite element mesh. The global *cycle jump* is then determined for the whole finite element mesh as a certain percentile of the cumulative relative frequency distribution of all local *cycle jump* values. Figure 6 illustrates the *cycle jump* principle applied to tension-compression loading.

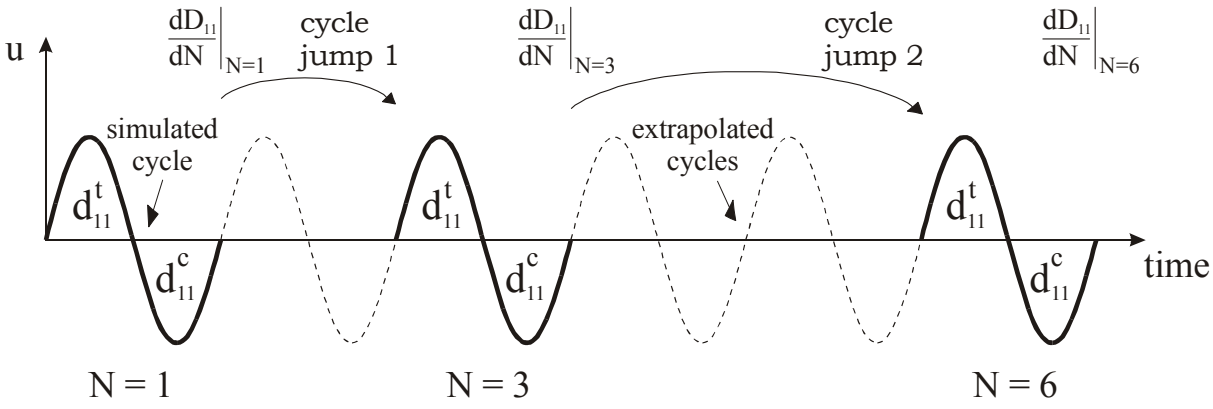

Figure 6 The *cycle jump* approach for tension-compression loading.

The last problem in the exposed modelling approach for tension-compression loading is the "crack closure" problem. This phenomenon was already encountered by Lemaitre when he defined the effective stress concept [23]. He observed that the effective stress $\tilde{\sigma}$ should be different in tension and compression tests on concrete specimens for two important reasons [24]:

- static rupture was different in tension and compression,
- the elasticity modulus was different in tension and compression.

These effects are associated with crack closure. Due to the closure of micro-cracks and micro-cavities in compression, the ability of the cross-section to carry loads depends upon the sign of the applied stress. Lemaitre suggested to define the effective stress in the one-dimensional case as follows [24]:

$$\tilde{\sigma} = \frac{\sigma}{1-D} \quad \text{if} \quad \sigma \geq 0$$
$$\tilde{\sigma} = \frac{\sigma}{1-hD} \quad \text{if} \quad \sigma < 0 \tag{6}$$

where h is a closure coefficient which characterizes the closure of the micro-cracks and micro-cavaties. Lemaitre concluded from experimental results that h = 0.2 is an acceptable value for several materials. Later on Lemaitre translated the concept to the three-dimensional case for quasi-static loading of metals [25].

It is important to note that the damage variable D in the definition by Lemaitre is the damage caused by tensile stresses in concrete. For concrete, it was assumed that the damage caused by compressive stresses was negligible. Here the effective stress must be transformed into:

$$\tilde{\sigma} = \frac{\sigma}{1-(d_{11}^t + d_{11}^c)} \quad \text{if } \sigma \geq 0$$
$$\tilde{\sigma} = \frac{\sigma}{1-(d_{11}^c + h\, d_{11}^t)} \quad \text{if } \sigma < 0 \tag{7}$$

The value of 0.2 for the crack closure coefficient has been retained for all subsequent calculations. It is important to note that through this definition, the fatigue failure index Σ becomes a function of σ, d_{11}^t and d_{11}^c.

Now that the global framework for the modelling approach of the tension-compression fatigue loading conditions has been explained, the modified growth rate equations will be discussed.

Growth rate equations for tension-compression fatigue loading

From Figure 3 and Figure 4, it is clear that the additional damage mechanisms due to fully-reversed bending, are much more damage-driven than stress-driven, even though no delaminations are present. The imposed displacement u_{max} is so small that the induced stresses and strains are very small compared to the static strengths in tension and compression. The damage growth rate equations of the originally proposed model are governed by the fatigue failure index $\Sigma(\sigma, D)$, but when applied to the fully-reversed bending experiment, the degradation is very small and seriously underestimates the real damage growth.
Moreover there is numerous evidence in open literature that tension-compression fatigue is more detrimental than tension-tension fatigue, even without delaminations. Two major reasons can be distinguished: increased debond growth and crack closure phenomena.
Very recently Gamstedt and Sjögren [22] have published a sound theory to explain the increased debond growth with tension-compression fatigue. They observed that, when a debond is subjected to compressive loading, an opening zone appears at the tips of the interfacial crack. Since debond propagation is more susceptible to mode I loading, the debond growth rate will be larger in compression. Indeed, for global tension, crack propagation would be in pure shear mode because the crack tip is closed. They further showed that debonding is the initiating mechanism to transverse cracking.
Once the transverse cracks have been initiated, crack closure phenomena play an important role as well. Wevers et al. [26][27] proved that during the growth of 90° cracks in $[0_2/90_2]_s$ carbon epoxy composites, material debris is formed between the crack faces. When the crack is closed, this excess of material causes compressive forces in the 90° plies for perpendicular cracks, or sliding forces for inclined matrix cracks. Thus, due to crack closure, additional damage is introduced.
The fatigue damage model which was proposed for single-sided bending, will now be extended to include the damaging effect of tension-compression fatigue loading. Thereto the differential growth rate equations for tensile damage d_{11}^t and compressive damage d_{11}^c will be coupled.

Damage initiation function

As reported by Gamstedt and Sjögren [22], there is an accelerated initiation of transverse cracks under tension-compression loading. They observed that the total length of transverse cracks grew to be more than twice as large for tension-compression compared to tension-tension. This is confirmed by the present bending fatigue experiments. When the decrease of the bending force during the first 2,200 cycles is calculated for several bending fatigue experiments, it appears that the force difference ΔF is considerably larger for fully-reversed bending than for single-sided bending. In Table 3, some values are presented, and although there is some scatter on the ΔF value, it clearly shows that the damage initiation phase is more damaging for fully-reversed bending.

Table 3 Degradation of bending force during first 2,200 loading cycles.

Single-sided bending			Fully-reversed bending		
Specimen	u_{max}	ΔF (N=2,200)	Specimen	u_{max}	ΔF (N=2,200)
Pr08_2	39.0 mm	7.33 N			
Pr10_4	34.4 mm	5.68 N			
Pr05_3	29.5 mm	5.21 N			
Pr05_1	27.7 mm	3.30 N	Pr08_6	27.0 mm	6.21 N
			Pr09_5	21.8 mm	3.29 N
			Pr08_4	19.5 mm	4.53 N

Hence the model constants c_1 and c_2 in Eq. (5) should be affected by the transition to tension-compression loading. However, as a sound modelling requires a constant value of the parameters c_1 and c_2 for both single-sided and fully-reversed loading, the constants c_1 and c_2 are not modified themselves, but are multiplied with a damage-dependent function. The first function should increase the parameter c_1, because the initiation rate for reversed loading is higher, while the second function should decrease the parameter c_2, because the saturation state is reached at a higher matrix crack density. Nevertheless, the introduction of these functions alone did not suffice to simulate the accelerated initiation phase satisfactorily. From a detailed inspection of the model equations, it was proved that the third power of the damage initiation function for compressive stresses (Eq. (5)) should decrease to simulate the accelerated damage initiation phenomenon adequately. Indeed, when the third power is maintained for fully-reversed bending, the compressive damage remains very small, and the resulting bending force degradation remains limited, because the decreasing load-bearing capacity at the tensile side is compensated by higher stresses at the compressive side. However, when the third power is lowered, the damage initiation phase can be simulated very well. The new equations for the damage initiation phase with tension-compression fatigue loading are:

$$\begin{cases} \left.\dfrac{d(d_{11}^t)}{dN}\right|_{initiation} = c_1 \cdot \left(1+\left(d_{11}^c\right)^2\right) \cdot \Sigma \cdot \exp\left(-c_2 \dfrac{d_{11}^t}{\sqrt{\Sigma}\cdot\left(1+\left(d_{11}^c\right)^2\right)}\right) & \text{if } \sigma \geq 0 \\ \left.\dfrac{d(d_{11}^c)}{dN}\right|_{initiation} = \left[c_1 \cdot \left(1+\left(d_{11}^t\right)^2\right) \cdot \Sigma \cdot \exp\left(-c_2 \dfrac{d_{11}^c}{\sqrt{\Sigma}\cdot\left(1+\left(d_{11}^t\right)^2\right)}\right)\right]^{1+2\cdot\exp(-c_6\cdot d_{11}^t)} & \text{if } \sigma < 0 \end{cases} \quad (8)$$

Only one new constant c_6 has been introduced, which regulates the decrease of the third power and the accelerated initiation of compressive damage. It is worthwhile to note that if there is only one type of damage (compressive or tensile) in each material point, the equations reduce to the ones for single-sided bending (Eq. (5)).

Figure 7 shows the force-cycle history of the Pr08_4 specimen for the first 150,000 loading cycles under fully-reversed bending, together with two finite element simulations. The first simulation used the coupled equations for damage initiation in Eq. (8), while the second simulation used the uncoupled terms for damage initiation under single-sided bending in Eq. (5). The displacement ratio R_d was –1.0 and u_{max} was 19.5 mm. The constant c_6 was optimized to be 13.0, while the other constants c_1 and c_2 were retained (see Table 2).

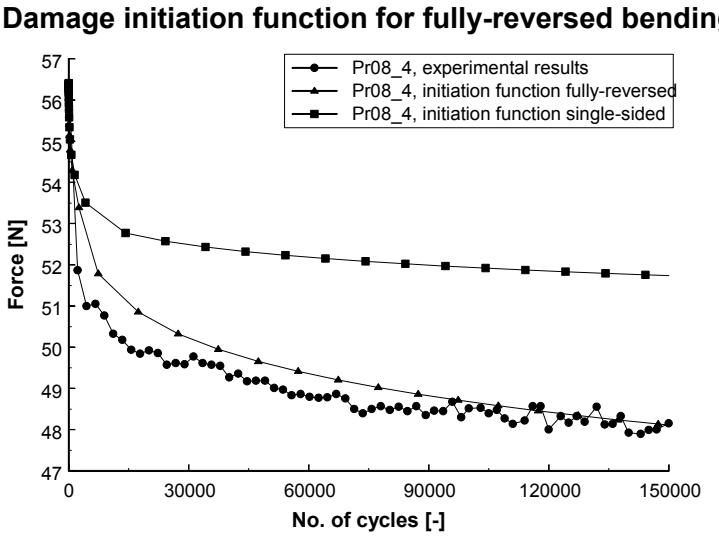

Figure 7 **Damage initation for fully-reversed bending with uncoupled and coupled growth rate equations.**

Damage propagation function

It appears from Figure 3 that the slope of the second stage of the force-cycle history is increased for fully-reversed bending. This has also been observed with other fatigue experiments: the downhill slope of the force-cycle history for the fully-reversed bending experiments is larger than for the single-sided bending experiments. Therefore it seems evident that also the second term in the growth rate equations which accounts for damage propagation, should be increased.
For single-sided bending, damage propagation was accelerated fast as soon as the threshold c_4 was crossed (initiation of fibre fracture leading to final failure). From various simulations, it appeared that for fully-reversed bending, the damage propagation is also accelerated by the presence of the other type of damage (d_{11}^t or d_{11}^c), but only if a certain threshold for the fatigue failure index $\Sigma(\sigma,\ d_{11}^t,\ d_{11}^c)$ has been crossed. Hence the damage propagation term in Eq. (5) is replaced by:

$$\begin{cases} \left.\dfrac{d(d_{11}^t)}{dN}\right|_{propagation} = c_3 \cdot d_{11}^t \cdot \Sigma^2 \cdot \left[1+\dfrac{\sqrt{d_{11}^c}\exp\left(c_8\sqrt{d_{11}^c}\right)}{1+\exp\left(-c_5(\Sigma-c_7)\right)}\right]\cdot\left[1+\exp\left(c_5(\Sigma-c_4)\right)\right] & \text{if } \sigma \geq 0 \\ \left.\dfrac{d(d_{11}^c)}{dN}\right|_{propagation} = c_3 \cdot d_{11}^c \cdot \Sigma^2 \cdot \left[1+\dfrac{\sqrt{d_{11}^t}\exp\left(c_8\sqrt{d_{11}^t}\right)}{1+\exp\left(-c_5(\Sigma-c_7)\right)}\right]\cdot\left[1+\exp\left(\dfrac{c_5}{3}(\Sigma-c_4)\right)\right] & \text{if } \sigma < 0 \end{cases} \quad (9)$$

Although this new damage acceleration factor may seem complicated, it simply expresses that due to the mutual interaction of both damage types, the damage propagation term is multiplied with the factor $[1+\sqrt{d_{11}^c}\exp(c_8\sqrt{d_{11}^c})]$ or $[1+\sqrt{d_{11}^t}\exp(c_8\sqrt{d_{11}^t})]$, once the fatigue failure index $\Sigma(\sigma,\ d_{11}^t,\ d_{11}^c)$ has crossed the threshold c_7. The presence of this threshold c_7 is modelled

by the sigmoidal function $1/[1+\exp(-c_5(\Sigma-c_7))]$. This function is widely used in neural networking algorithms, where it behaves as an activation function in each node of the neural network topology. Here it acts in the same way: once that the fatigue failure index $\Sigma(\sigma, d_{11}^t, d_{11}^c)$ has crossed the threshold c_7, damage propagation will be accelerated due to the presence of the other damage type (d_{11}^t or d_{11}^c). Figure 8 shows the behaviour of the sigmoidal function, the constants c_5 and c_7 being 93.0 (see Table 2) and 0.5, respectively.

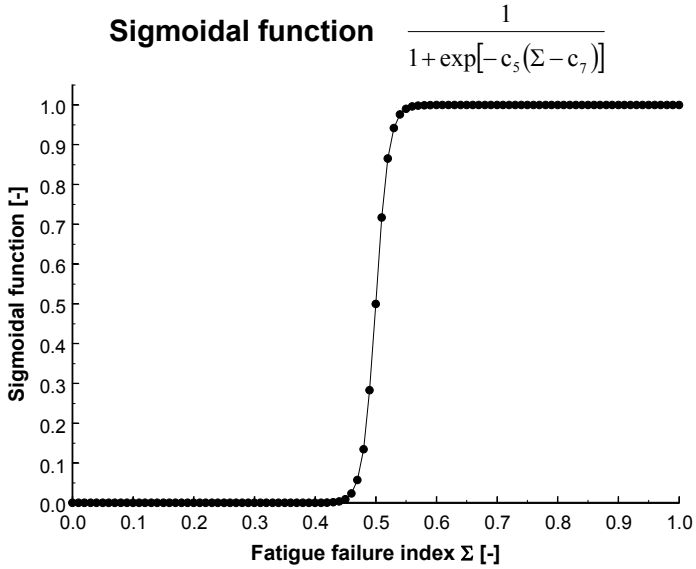

Figure 8 Sigmoidal function used to model the threshold existence.

Although it seems from Eq. (9) that, once the threshold c_7 has been crossed, the damage acceleration factor depends no longer on the actual value of the fatigue failure index Σ, this is not the case. If the fatigue failure index Σ increases, the increased growth rates $d(d_{11}^t)/dN$ and $d(d_{11}^c)/dN$ will contribute to a higher value of d_{11}^t and d_{11}^c, and hence to a larger value of the coupled damage acceleration factors.

Again the system of equations (Eq. 9) reduces to the original model for single-sided bending, when only one type of damage is present in each material point. Further it is important to note that even if the fatigue failure index Σ is below the damage acceleration threshold c_7, there is still a coupling between the two expressions $d(d_{11}^t)/dN$ and $d(d_{11}^c)/dN$ for damage propagation, because the fatigue failure index is function of the effective stress $\tilde{\sigma}$ and this effective stress $\tilde{\sigma}$ accounts for both tensile and compressive damage (Eq. (7)).

Final layout of the fatigue damage model

The final system of damage growth rate equations can be written as:

$$\begin{cases} \dfrac{d(d_{11}^t)}{dN} = c_1 \cdot \left(1+\left(d_{11}^c\right)^2\right) \cdot \Sigma \cdot \exp\left(-c_2 \dfrac{d_{11}^t}{\sqrt{\Sigma} \cdot \left(1+\left(d_{11}^c\right)^2\right)}\right) & \text{if } \sigma \geq 0 \\ \qquad + c_3 \cdot d_{11}^t \cdot \Sigma^2 \cdot \left[1+\dfrac{\sqrt{d_{11}^c}\,\exp\left(c_8\sqrt{d_{11}^c}\right)}{1+\exp\left(-c_5(\Sigma-c_7)\right)}\right] \cdot \left[1+\exp\left(c_5(\Sigma-c_4)\right)\right] & \\ \dfrac{d(d_{11}^c)}{dN} = \left[c_1 \cdot \left(1+\left(d_{11}^t\right)^2\right) \cdot \Sigma \cdot \exp\left(-c_2 \dfrac{d_{11}^c}{\sqrt{\Sigma} \cdot \left(1+\left(d_{11}^t\right)^2\right)}\right)\right]^{1+2\cdot\exp\left(-c_6 \cdot d_{11}^t\right)} & \text{if } \sigma < 0 \\ \qquad + c_3 \cdot d_{11}^c \cdot \Sigma^2 \cdot \left[1+\dfrac{\sqrt{d_{11}^t}\,\exp\left(c_8\sqrt{d_{11}^t}\right)}{1+\exp\left(-c_5(\Sigma-c_7)\right)}\right] \cdot \left[1+\exp\left(\dfrac{c_5}{3}(\Sigma-c_4)\right)\right] & \\ D_{11} = d_{11}^t + d_{11}^c & \end{cases} \quad (10)$$

As compared to the fatigue damage model for single-sided bending, three additional constants c_6, c_7 and c_8 have been introduced. Each of these constants has again a very close relation with the underlying damage mechanisms. The constant c_6 expresses the experimental observation that damage initiation in the compressive regime is accelerated by the presence of tensile damage, as reported by Gamstedt and Sjögren [22]. The constants c_7 and c_8 are introduced in the damage acceleration factor, which simulates that once the fatigue failure index Σ has crossed the threshold c_7, the damage propagation is accelerated because of the presence of the other damage type (d_{11}^t or d_{11}^c). Of course, the constants c_i (i=1,…,5) keep their values listed in Table 2.

FINITE ELEMENT SIMULATIONS

The three constants c_6, c_7 and c_8 have been determined for the fully-reversed bending fatigue test Pr08_4. The imposed displacement amplitude u_{max} was 19.5 mm and the displacement ratio R_d was equal to –1.0 (fully-reversed bending). In Figure 9, the experimental and simulated results are shown. The constants c_6, c_7 and c_8 were determined to be respectively: 13.0 [-], 0.5 [-] and 9.7 [-]. The constants c_i (i = 1,…,8) were of course retained for all subsequent simulations.

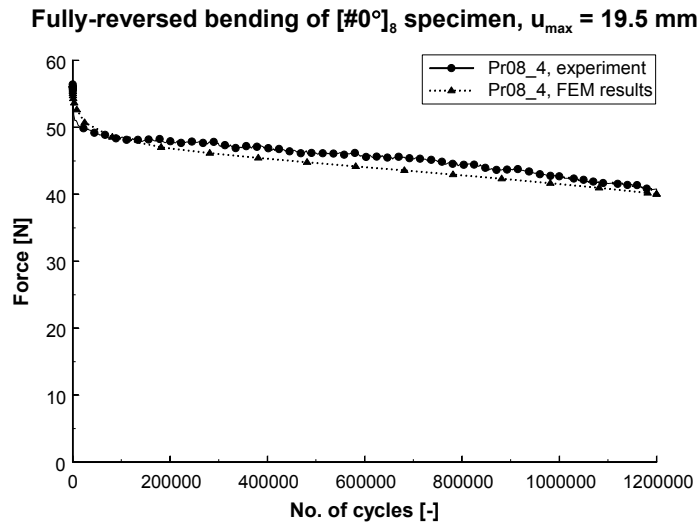

Figure 9 Experimental and simulated results for a $[\#0°]_8$ specimen with u_{max} = 19.5 mm and R_d = -1.0.

It is worthwhile to note that there is indeed a threshold for damage propagation, because the fatigue life now exceeds 1,200,000 cycles for u_{max} = 19.5 mm, while it was reduced to about 70,000 cycles for the fatigue test Pr08_6 with u_{max} = 27.0 mm (see Figure 3). Figure 10 shows the experimental and simulated force-cycle history for this Pr08_6 specimen. The fatigue damage model simulates the observed experimental behaviour satisfactorily, the more so as the material constants c_i (i = 6,7,8) were optimized for a fatigue life of more than 1,200,000 cycles.

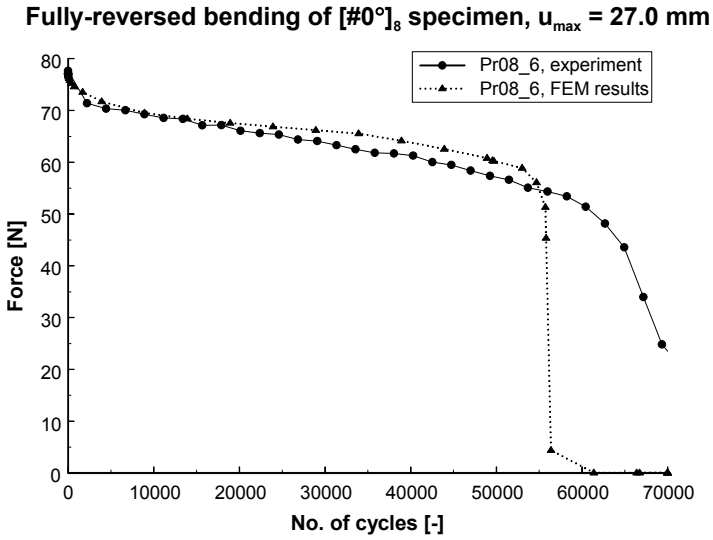

Figure 10 Experimental and simulated results for a $[\#0°]_8$ specimen with u_{max} = 27.0 mm and R_d = -1.0.

It was stated earlier that the stress ratio R (= $\sigma_{min}/\sigma_{max}$) is not a suitable parameter to describe the fatigue loading conditions in the tension-compression regime. This can be clearly demonstrated by the simulated results of this last fatigue test. The Gauss-point 1602 was

chosen as the point of interest as it is lying at the specimen surface in the clamped cross-section. Figure 11 schematically shows its position in the finite element mesh.

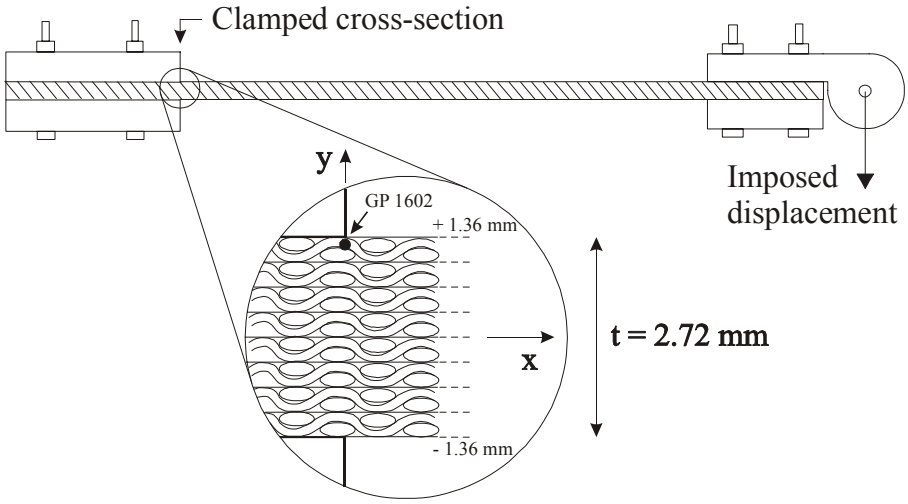

Figure 11 Position of the Gauss-point of interest in the clamped cross-section.

In Figure 12 the time-history of the nominal stress σ_{11} for this particular Gauss-point is shown at several stages of fatigue life. The fatigue test frequency was mentioned to be 2.2 Hz, so one fatigue cycle corresponds to 0.45 seconds. At the first loading cycle, the Gauss-point is loaded with a tensile stress during the first half of the period and with an equal compressive stress during the second half of the period. The stress ratio R is indeed –1.0. However when damage is initiating, the stress magnitudes diverge for tension and compression, because the damage growth rate expressions are different and the compression-loaded specimen side is behaving stiffer due to the crack closure phenomenon (see Equation (7)). So the stress ratio R is continuously changing during fatigue life, as is the general case in real structures. At cycle 33,918, the stress ratio R for this particular Gauss-point has become –1.7 (= -134.8/79.2), while the stress ratio R was –1.0 for the first loading cycle.

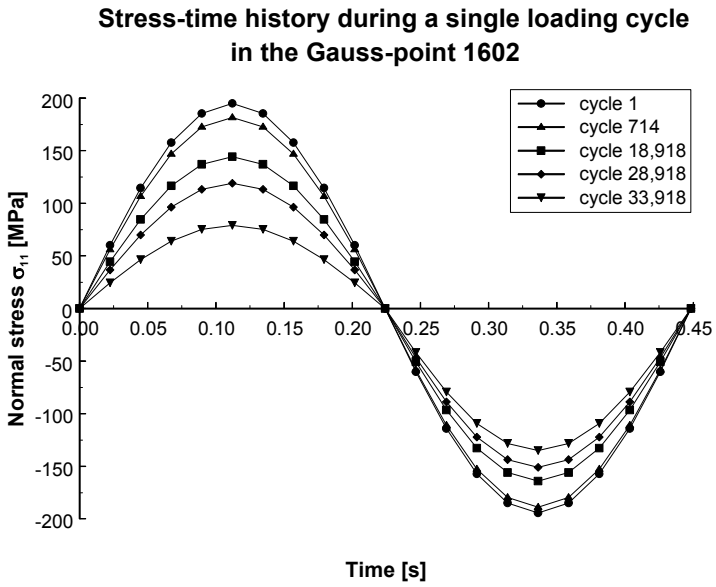

Figure 12 Stress-time history during one single fatigue loading cycle for a particular Gauss-point.

Finally, Figure 13 shows for the same Gauss-point 1602 the evolution of the total damage D_{11}, the tensile damage d_{11}^t and the compressive damage d_{11}^c.

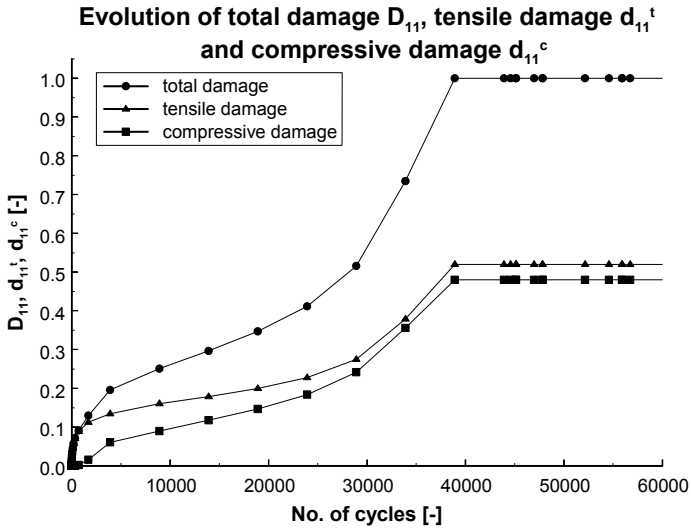

Figure 13 Evolution of total, tensile and compressive damage in a particular Gauss-point.

It is worthwhile to note that although the Gauss-point 1602 is predicted to fail at cycle 38,918 (and thus also the Gauss-point at the reverse surface of the specimen), the bending force is maintained for 17,000 cycles more at a relatively high level. This is of course due to the stress redistribution in the cross-sections near the clamped end of the composite specimen, as illustrated by Figure 14.

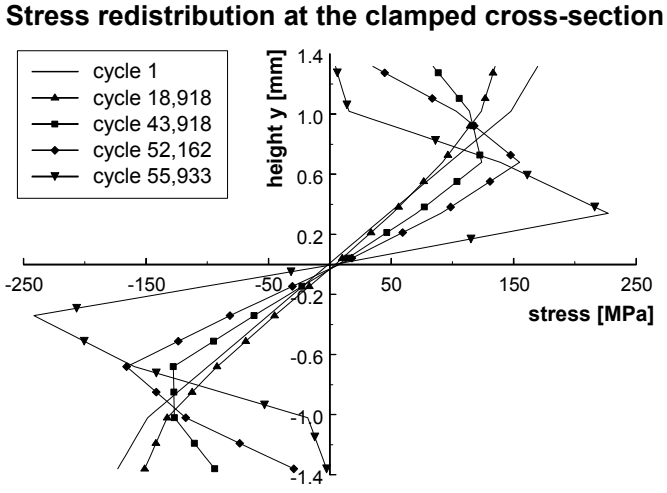

Figure 14 Stress redistribution at the clamped cross-section during fatigue life.

The last simulation is for the specimen Pr09_5. This specimen was subjected to a slightly larger displacement amplitude u_{max} = 21.8 mm than the Pr08_4 experiment (see Figure 9). In Figure 15, the experimental and simulated results are shown.

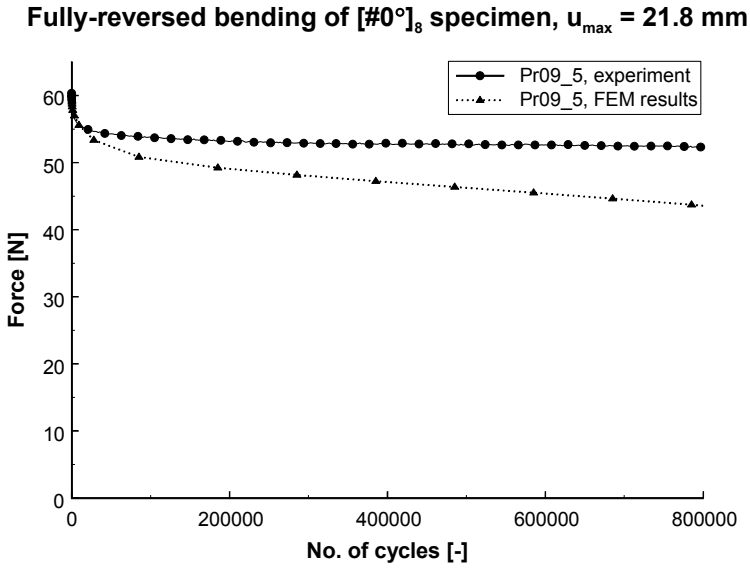

Figure 15 Experimental and simulated results for a $[\#0°]_8$ specimen with u_{max} = 21.8 mm and R_d = -1.0.

It appears that the degradation is overpredicted by the fatigue damage model. This is not surprising, because it could already be seen from Table 3 that the Pr09_5 specimen shows a smaller initial decline of the bending force than the other specimens. After the initial decline, the experimental force-cycle history remains almost horizontal, while there was a significant slope in the force-cycle history of the Pr08_4 specimen (see Figure 9) although the latter was subjected to a smaller displacement amplitude u_{max}. This proves that the value of the threshold for damage propagation is subject to some experimental scatter, but this is an intrinsic property of fatigue experiments.

CONCLUSIONS

A fatigue damage model for simulation of tension-compression fatigue loadings has been proposed. The innovative aspects of the model are: (i) through the modified use of the static Tsai-Wu failure criterion, there is a correlation between residual stiffness and strength. Nevertheless the complete framework of the model is consistent with the continuum damage mechanics theory; (ii) the stress ratio R as a characterization of tension-compression fatigue tests has been replaced by a coupled system of growth rate equations for tensile and compressive damage. This approach is far more general in nature than the stress ratio R, as it can keep track of stress redistributions during fatigue life (which implies varying stress ratios); (iii) the model has been implemented in a commercial finite element code and hence allows for simulation of the fatigue behaviour of more complex composite components.
The model has been validated by finite element simulations of displacement-controlled bending fatigue experiments on plain woven glass/epoxy specimens. The cycle-history of the bending force, damage variables and stress components could be simulated satisfactorily.

ACKNOWLEDGEMENTS

The author W. Van Paepegem gratefully acknowledges his finance through a grant of the Fund for Scientific Research – Flanders (F.W.O.), and the advice and technical support of the SAMTECH company. The authors also express their gratitude to Syncoglas for their support and technical collaboration.

REFERENCES

[1]	Carmet, A., Weber, B. and Robert, J.L. (2000). Fatigue Life Assessment of Components and Structures Under Multiaxial Service Loading. In : Bache, M.R. et al. (eds.). Fatigue 2000 : Fatigue & Durability assessment of materials, components and structures. Proceedings. Cambridge, 10-12 April 2000, Chameleon Press Ltd., pp. 295-304.
[2]	Degrieck, J. and Van Paepegem, W. (2001). Fatigue Damage Modelling of Fibre-Reinforced Composite Materials: Review. Applied Mechanics Reviews, 54(4), 279-300.
[3]	Van Paepegem, W. and Degrieck, J. (2001). Experimental setup for and numerical modelling of bending fatigue experiments on plain woven glass/epoxy composites. Composite Structures, 51(1), 1-8.
[4]	Van Paepegem, W. and Degrieck, J. (2000). Numerical modelling of fatigue degradation of fibre-reinforced composite materials. In: Topping, B.H.V. (ed.). Proceedings of the Fifth International Conference on Computational Structures Technology. Volume F: Computational Techniques for Materials, Composites and Composite Structures, Leuven, 6-8 September 2000, Civil-Comp Press, pp. 319-326.
[5]	Salkind, M.J. (1972). Fatigue of composites. In: Corten, H.T. (ed.). Composite Materials Testing and Design (Second Conference). ASTM STP 497. Baltimore, American Society for Testing and Materials, pp. 143-169.
[6]	Hahn, H.T. and Kim, R.Y. (1976). Fatigue behaviour of composite laminates. Journal of Composite Materials, 10, 156-180.
[7]	O'Brien, T.K. and Reifsnider, K.L. (1981). Fatigue damage evaluation through stiffness measurements in boron-epoxy laminates. Journal of Composite Materials, 15, 55-70.
[8]	Hwang, W. and Han, K.S. (1986). Cumulative damage models and multi-stress fatigue life prediction. Journal of Composite Materials, 20, 125-153.
[9]	Sol, H. and de Wilde, W.P. (1988). Identification of elastic properties of composite materials using resonant frequencies. In : Brebbia, C.A., de Wilde, W.P. and Blain, W.R. (eds.). Proceedings of the International Conference "Computer Aided Design in Composite Material Technology", Southampton, 1988, Springer-Verlag, pp. 273-280.
[10]	Sol, H. (1990). Identification of the complex moduli of composite materials by a mixed numerical/experimental method. In : de Wilde, W.P. and Blain, W.R. (eds.). Proceedings of the second International Conference on Computer Aided Design in Composite Material Technology, Brussels, 25-27 April 1990, Springer-Verlag, pp. 267-279.
[11]	Van Paepegem, W. and Degrieck, J. (2001). New coupled coupled approach of residual stiffness and strength for fatigue of fibre-reinforced composites. Eight International Conference on Composites Engineering (ICCE/8). Proceedings. Tenerife, 5-11 August 2001.
[12]	Van Paepegem, W. and Degrieck, J. (2001). A New Coupled Approach of Residual Stiffness and Strength for Fatigue of Fibre-reinforced Composites. Accepted for publication in International Journal of Fatigue.

[13]	Liu, K.-S. and Tsai, S.W. (1998). A progressive quadratic failure criterion for a laminate. Composites Science and Technology, 58, 1023-1032.
[14]	Schulte, K. (1984). Stiffness reduction and development of longitudinal cracks during fatigue loading of composite laminates. In : Cardon, A.H. and Verchery, G. (eds.). Mechanical characterisation of load bearing fibre composite laminates. Proceedings of the European Mechanics Colloquium 182, 29-31 August 1984, Brussels, Belgium, Elsevier, pp. 36-54.
[15]	Highsmith, A.L. and Reifsnider, K.L. (1982). Stiffness-reduction mechanisms in composite laminates. In : Reifsnider, K.L. (ed.). Damage in composite materials. ASTM STP 775. American Society for Testing and Materials, pp. 103-117.
[16]	Masters, J.E. and Reifsnider, K.L. (1982). An investigation of cumulative damage development in quasi-isotropic graphite/epoxy laminates. In : Reifsnider, K.L. (ed.). Damage in composite materials. ASTM STP 775. American Society for Testing and Materials, pp. 40-62.
[17]	Van Paepegem, W., Degrieck, J. and De Baets, P. (2001). Finite Element Approach for Modelling Fatigue Damage in Fibre-reinforced Composite Materials. Composites Part B, 32(7), 575-588.
[18]	Bartley-Cho, J., Lim, S.G., Hahn, H.T. and Shyprykevich, P. (1998). Damage accumulation in quasi-isotropic graphite/epoxy laminates under constant-amplitude fatigue and block loading. Composites Science and Technology, 58, 1535-1547.
[19]	Gathercole, N., Reiter, H., Adam, T. and Harris, B. (1994). Life prediction for fatigue of T800/5245 carbon-fibre composites: I. Constant-amplitude loading. International Journal of Fatigue, 16(8), 523-532.
[20]	Adam, T., Gathercole, N., Reiter, H. and Harris, B. (1994). Life prediction for fatigue of T800/5245 carbon-fibre composites: II. Variable-amplitude loading. International Journal of Fatigue, 16(8), 533-547.
[21]	Badaliance, R., Dill, H.D. and Potter, J.M. (1982). Effects of spectrum variations on fatigue life of composites. In : Daniel, I.M. (ed.). Composite materials : Testing and design (Sixth Conference). ASTM STP 787. Philadelphia, American Society for Testing and Materials, pp. 274-286.
[22]	Gamstedt, E.K. and Sjogren, B.A. (1999). Micromechanisms in tension-compression fatigue of composite laminates containing transverse plies. Composites Science and Technology, 59(2), 167-178.
[23]	Lemaitre, J. (1971). Evaluation of dissipation and damage in metals, submitted to dynamic loading. Proceedings I.C.M. I, Kyoto, Japan.
[24]	Krajcinovic, D. and Lemaitre, J. (eds.) (1987). Continuum damage mechanics: theory and applications. Wien, Springer - Verlag, 294 pp.
[25]	Lemaitre, J., Desmorat, R. and Sauzay, M. (2000). Anisotropic damage law of evolution. European Journal of Mechanics A/Solids, 19, 187-208.
[26]	Wevers, M., Verpoest, I., Aernoudt, E. and De Meester, P. (1987). Fatigue damage development in carbon fibre reinforced epoxy composites: correlation between the stiffness degradation and the growth of different damage types. In : Matthews, F.L., Buskell, N.C.R., Hodgkinson, J.M. and Morton, J. (eds.). Sixth International Conference on Composite Materials (ICCM-VI) & Second European Conference on Composite Materials (ECCM-II) : Volume 4. Proceedings, 20-24 July 1987, London, UK, Elsevier, pp. 4.114-4.128.
[27]	Wevers, M., Verpoest, I. and De Meester, P. (1990). Is crack closure due to fatigue loading causing more damage in carbon fibre reinforced epoxy composites ? In : Füller, J., Grüninger, G., Schulte, K., Bunsell, A.R. and Massiah, A. (eds.). Developments in the science and technology of composite materials. Proceedings of the Fourth European Conference on Composite Materials (ECCM/4), 25-28 September 1990, Stuttgart, Elsevier Applied Science, pp. 181-188.